Impact of turbulence-induced asymmetric propagators on the accuracy of phase-contrast velocimetry

Impact of turbulence-induced asymmetric propagators on the accuracy of Phase-contrast Velocimetry.

Haitham F.I. Al-Mubarak[1,3] Antoine Vallatos[1,2] and William M. Holmes[1*]

[1] Glasgow Experimental MRI Centre, Institute of Neuroscience and Psychology, University of Glasgow, UK.

[2] Centre for Clinical Brain Sciences, University of Edinburgh, UK.

[3] Department of Physics, College of Science, Misan university, Iraq

* Corresponding author:

Name William M. Holmes

Department Glasgow Experimental MRI Centre

Institute Institute of Neuroscience and Psychology

Address University of Glasgow, Wellcome Surgical Centre, Garscube Estate, Bearsden Road, Glasgow G611QH, UK.

E-mail william.holmes@glasgow.ac.uk.

Keywords: velocity imaging, velocimetry, phase-shift velocimetry, phase-contrast velocimetry, propagator, flow, displacement distribution, wall shear stress, turbulence,

Manuscript word count:

Abstract word count:

Abstract

Phase-contrast magnetic resonance velocimetry (PC-MRI) has been widely used to investigate flow properties in numerous systems. In a horizontal cylindrical pipe (3mm diameter), we investigated the accuracy of PC-MRI as the flow transitioned from laminar to turbulent flow (Reynolds number 352 to 2708). We focus primarily on velocimetry errors introduced by skewed intra-voxel displacement distributions, a consequence of PC-MRI theory assuming symmetric distributions. We demonstrated how rapid fluctuations in the velocity field, can produce broad asymmetric intravoxel displacement distributions near the wall. Depending on the shape of the distribution, this resulted in PC-MRI measurements under-estimating (positive skewness) or over-estimating (negative skewness) the true mean intravoxel velocity, which could have particular importance to clinical wall shear stress measurements. The magnitude of these velocity errors was shown to increase with the variance and decrease with the kurtosis of the intravoxel displacement distribution. These experimental results confirm our previous theoretical analysis, which gives a relationship for PC-MRI velocimetry errors, as a function of the higher moments of the intravoxel displacement distribution (skewness, variance, and kurtosis) and the experimental parameters q and Δ. This suggests that PC-MRI errors in such unsteady/turbulent flow conditions can potentially be reduced by employing lower q values or shorter observation times Δ.

1. Introduction

The ability of Magnetic Resonance Imaging to non-invasively map flow fields has found important clinical (1) and research applications (2). The use of pulsed field gradient nuclear magnetic resonance (PFG-NMR) for velocimetry was first reported by Hayward *et. al.* (3) in 1972. Ten years later, Moran (4) described a theoretical method for velocity imaging. Subsequent developments led to the phase difference technique known today as phase-contrast MRI (PC-MRI) (5,6). PC-MRI is widely used to image pulsatile blood flow through the heart and great vessels, where turbulence is seen in both healthy and diseased states (7). The pathogenesis of various cardiovascular diseases is associated with turbulent blood flow (8-10). The intensity of such turbulent velocity fluctuations has been estimated via the NMR signal attenuation (11), time-averaged imaging(12) and clinically via intravoxel velocity standard deviation (IVSD) mapping (13). The accuracy of PC-MRI when studying laminar flows has been thoroughly demonstrated, though less so for unsteady and turbulent flows. Efforts have been made to compare PC-MRI measurements with Laser-Doppler (14-16) particle image velocimetry (PIV)(17-20) and numerically simulated flow data (21-23).

An often overlooked assumption made in the theory of PC-MRI is that the intravoxel displacement distributions (propagators) are symmetric (24,25). This assumption is generally valid for simple laminar flows, but is not necessarily valid for complex flows, such as flow through porous media (26). In a recent work, we described theoretically how the higher order moments (variance, skewness, kurtosis, see Figure 1b,c) of the displacement distribution can severely affect the accuracy of PC-MRI (27), causing both under-estimation (positive skewness cases) and over-estimation (negative skewness cases) of the true mean velocity. This type of error depends critically on non-zero skewness, with the magnitude of the error increasing with the both the skewness and variance of the distribution. This was verified experimentally with steady (non-fluctuating) flow fields, using phantoms (28) and flow through rocks (26).

Here we consider intravoxel displacement distributions produced by temporally fluctuating flow fields, (i.e. turbulent flow). For these experiments, we returned to the simplest and most studied geometry, namely non-pulsatile flow through a horizontal pipe. Reynolds et al. (29) first investigated the transition to turbulence in straight pipe flow, which can be described by a single dimensionless parameter, the Reynolds number, $Re = QD/vA$, where Q is the volumetric flow rate, D the pipe diameter, v the kinematic viscosity and A the pipe cross-section area. In pipe flow, for a Newtonian fluid, the transition from laminar flow to turbulent flow is characterised by a Reynolds number of approximately Re~2000 (30). Here high quality displacement distributions were acquired using Fourier Flow Imaging (FFI) with 64 q values (31), from which the higher order moments could be directly mapped. As the FFI measured mean velocities are independent of the shape of the intravoxel displacement distribution, these are used as a ground truth with which to assess the accuracy of PC-MRI. Errors in PC-MRI are then explained theoretically in terms of the higher order moments of the intravoxel displacement distribution.

2. Theory

PFG NMR velocimetry consists of making the Nuclear Magnetic Resonance (NMR) signal sensitive to translational motion by applying a magnetic field gradient of amplitude G and duration δ, which imposes a spatially dependent phase to each nuclear spin of gyromagnetic ratio γ. For a spin moving along the path $\boldsymbol{r}(t)$, the induced phase is expressed as

$$\varphi(t) = \gamma \int_0^t \boldsymbol{G}(t) \cdot \boldsymbol{r}(t) dt. \qquad (1)$$

After an observation time Δ, a rephasing gradient is applied. For a spin starting at $\boldsymbol{r_0}$ and ending at $\boldsymbol{r_0 + R}$, the resulting phase-shift is then given by $\boldsymbol{q \cdot R}$, with $\boldsymbol{q} = \gamma\delta\boldsymbol{G}$. In the narrow pulse approximation, $\delta \ll \Delta$, the overall signal resulting from a spatially resolved PFG NMR experiment can be expressed as

$$S(\boldsymbol{k},\boldsymbol{q}) = \iint \rho(\boldsymbol{r})P_{\Delta}(\boldsymbol{R},\boldsymbol{r})e^{i\boldsymbol{k}\cdot\boldsymbol{r}}e^{i\boldsymbol{q}\cdot\boldsymbol{R}}d\boldsymbol{r}d\boldsymbol{R}, \qquad (2)$$

where $\rho(\boldsymbol{r})$ is the spin density and $P_{\Delta}(\boldsymbol{R},\boldsymbol{r})$ the normalised probability distribution function for a spin with displacement $\boldsymbol{R}$ during Δ, also called a propagator. Defining the average velocity of each spin during Δ as $\bar{v} = R/\Delta$, it is possible to rewrite equation 2 as

$$S(\boldsymbol{k},\boldsymbol{q}) = \iint \rho(\boldsymbol{r})P_{\Delta}(\bar{v},\boldsymbol{r})e^{i\boldsymbol{k}\cdot\boldsymbol{r}}e^{i\boldsymbol{q}\cdot\bar{v}\Delta}d\boldsymbol{r}d\bar{v}. \qquad (3)$$

Fourier Flow Imaging (FFI), or propagator velocimetry, consists of acquiring $S(\boldsymbol{k},\boldsymbol{q})$ for a matrix of $\boldsymbol{k}$ and $\boldsymbol{q}$ values and then applying an inverse Fourier transform to obtain a spatially resolved velocity distribution. In each gradient direction, the number of q-steps and their size must be selected appropriately to cover the displacement range found in each voxel and obtain the desired propagator resolution.

Phase-Contrast Velocimetry (PC-MRI) seeks to measure only the average intravoxel velocity. For a given gradient direction, by inserting mean velocity, $V(\boldsymbol{r}) = \int \bar{v}P_{\Delta}(\bar{v},\boldsymbol{r})d\bar{v}$, into equation 3, one obtains

$$S(\boldsymbol{k},q) = \rho(\boldsymbol{r})e^{iqV(\boldsymbol{r})\Delta}\int P_{\Delta}(\bar{v},\boldsymbol{r})e^{iq(\bar{v}-V(\boldsymbol{r}))\Delta}d\bar{v}. \qquad (4)$$

Assuming the velocity probability distribution is symmetric around the average velocity $V(\boldsymbol{r})$, then the integral in equation 4 is real and the phase of the resulting signal is found to be proportional to $V(\boldsymbol{r})$ (5) and is given by

$$\varphi(\boldsymbol{r}) = q\Delta V(\boldsymbol{r}). \qquad (5)$$

By subtracting two phase images taken at equal Δ times, and with equal but opposite q values (q_2=-q_1) one can obtain a map with intensities proportional to velocity (32), expressed as

$$V(\boldsymbol{r}) = \frac{\varphi_2(\boldsymbol{r})-\varphi_1(\boldsymbol{r})}{(q_2-q_1)\Delta}. \qquad (6)$$

2.1 Theoretical relationship between velocimetry errors and higher order moments

To inform the following discussion it is helpful to review the moments of a distribution and give a qualitative description of their properties. For a displacement probability distribution $P_\Delta(R,r)$, the n^{th} moment of the distribution is

$$M_n = \int P_\Delta(R,r)\left(R - R_{average}\right)^n dR. \quad (7)$$

The first moment is termed the arithmetic mean of the distribution ($R_{average}$), the second moment the variance, the third moment the skewness and the fourth moment the kurtosis. The variance, being equal to the square of the standard deviation of the distribution, gives a measure of the amount of variation or dispersion in the distribution. The skewness is a measure of the asymmetry in the distribution about the mean, with a skewness of zero corresponding to a symmetric distribution. In the case of asymmetric distributions, the sign (+ or -) of the skewness indicates the side on which the tail of the distribution is more extended (e.g. Figure 1b). Finally, the kurtosis is a measure of the "tailedness/peakedness" of the distribution (e.g. Figure 1c).

In a previous work (27), we showed analytically how the error in PC-MRI measurements depends upon the higher order moments of the intravoxel displacement distribution. Taking the intravoxel velocity measured by the PC-MRI sequence as

$$V_{PCV}(\boldsymbol{r}) = V_{average}(\boldsymbol{r}) + V_{error}(\boldsymbol{r}), \quad (8)$$

where $V_{average}$ is the true average intravoxel velocity and V_{error} is an error term resulting from the higher moments in the displacement distribution. By substitution and Taylor expansion of equation 2, the V_{error} term can be written as a function of the intravoxel displacement distribution moments as

$$V_{error}(\boldsymbol{r}) = \frac{1}{q\Delta} tan^{-1}\left(\frac{-\frac{q^3}{3!}Skew\left(P_\Delta(R,\boldsymbol{r})\right)}{1-\frac{q^2}{2!}Var\left(P_\Delta(R,\boldsymbol{r})\right)+\frac{q^4}{4!}Kurt\left(P_\Delta(R,\boldsymbol{r})\right)}\right). \quad (9)$$

A full derivation and description can be found in Vallatos et al. (27).

Equation 9 is very useful in helping to understand how the shape of the intravoxel displacement distribution is related to the accuracy of PC-MRI. Despite its approximate character resulting from truncating an infinite Taylor series, this equation allows us to draw some important conclusions. First, the skewness of intravoxel displacement distribution has an important effect on the accuracy of PC-MRI measurements. V_{error} vanishes for $Skew\left(P_\Delta(R,\boldsymbol{r})\right) = 0$ (accurate mean velocity measurement),

becomes negative when $Skew\left(P_{\Delta}(R,\boldsymbol{r})\right) > 0$ (mean velocity under-estimation) and positive when $Skew\left(P_{\Delta}(R,\boldsymbol{r})\right) < 0$ (mean velocity over-estimation). Second, the error in PC-MRI measurements, V_{error}, increases with the variance of the displacement distribution.

3 Materials and Methods

3.1 MRI experiments

The MRI experiments were performed on a horizontal 7 tesla Bruker Pharmascan Avance III system (300 MHz). A Bruker BGA9 imaging gradient insert (300 mT m^{-1}) was used to provide linear magnetic field gradient pulses. A 72mm diameter birdcage RF coil was used to transmit and a 4-channel phase-array mouse brain coil was used to receive the signal.

Phase-Contrast Velocimetry (PC-MRI) and Fourier Flow Imaging (FFI) measurements were performed on water flow (1 g/L $CuSO_4$, T1 = 263 ms; T2 = 163 ms) through a long horizontal cylindrical pipe (silicone) of 3.0 mm inner diameter, with Reynolds numbers ranging from 352 to 2708. For the fastest flow rates used, the corresponding mean horizontal velocity was 1.07m/s. A reservoir of solution (250ml) was placed inside the magnet (Figure 1a), to allow sufficient time for full polarisation of the water before it flowed into the section of pipe that was to be imaged. Between the reservoir and the RF receiver coil there was a 0.7m straight section of piping.

PC-MRI measurements used a flow compensated gradient echo sequence [Bruker Flowmap, TE = 5 ms , TR = 20 ms, matrix 64 x 64, FOV 1.0 cm x 1.0 cm, gradient duration δ = 2ms , observation time Δ= 2ms, slice thickness 1mm, NA=2]. A threshold was applied to the magnitude image to identify the fluid filled voxels inside the pipe. Importantly, there was no ^1H signal observed from the pipe material. The corresponding FFI measurements were acquired using the same imaging parameters, except images were acquired for 64 q-values, evenly distributed around q = 0 m^{-1}. Displacement propagators, $P_{\Delta}(R,r)$, were obtained by normalisation of the inverse Fourier transform of the resulting signal against q. To obtain the high SNR propagators required to accurately determine the higher order moments, the FFI was acquired with NA=128, total scan time 1hour 30min. Measurements were made for a range of flow rates from 50 to 384 ml/min. The displacement distributions were divided by the observation time, Δ, to yield the velocity distribution $P_{\Delta}(v,r)$. For each voxel, the moments of the velocity distributions were calculated by numerical integration (trapezoidal method), yielding spatial maps of the mean, variance,

skewness and kurtosis. In addition, rapid serial PC-MRI measurements were made, acquiring 1000 repetitions with a temporal resolution of 1.9 sec.

4. Results

With the 3mm inner diameter pipe placed horizontally in the magnet, PC-MRI and Fourier Flowing Imaging measurements were taken for a range of flow rates, from laminar flow (Q=50ml/min, Re= 352), transition region (Q=261, Re =1840) and turbulent region (Q=384ml/min, Re= 2708).

4.1 Fourier Flow imaging (FFI).

3D inverse Fourier transformation of the acquired FFI data yields a "propagator" map, where each voxel has its own velocity probability distribution $P_{\Delta}(\boldsymbol{v}, \boldsymbol{r})$. Examples are shown in Figure 2b. For each voxel, the moments of the velocity distribution were calculated, yielding spatial maps of the mean, variance, skewness and kurtosis of the velocity distribution (Figure 3 a,b,c,d respectively).

Figure 3a shows maps of the mean velocity calculated from the FFI data. At low velocities (Q= 50ml/min and 137ml/min) the velocity profiles are parabolic, whereas at higher flow rates (transition to turbulence, Q=261ml/min and turbulent, Q=384ml/min) profiles are plug-like.

Figure 3b shows maps of variance calculated from the FFI data. At low velocities (Q= 50ml/min and 137ml/min) all the individual intravoxel velocity distributions $P_{\Delta}(\boldsymbol{v}, \boldsymbol{r})$ were narrow (low variance). At high flow rates (transition to turbulence, Q=261ml/min and turbulent, Q=384ml/min), a broad higher variance band was seen near wall, with low variance at the centre of the pipe.

Figure 3c shows maps of skewness calculated from FFI data. At low velocities (Q= 50ml/min and 137ml/min) all the individual intravoxel velocity distributions $P_{\Delta}(\boldsymbol{v}, \boldsymbol{r})$ are symmetric (Skewness ≈ 0). At high flow rates (transition to turbulence, Q=261ml/min and turbulent, Q=384ml/min), we found; a narrow ring with strong positive skewness adjacent to the wall; a second narrow ring, closer in, of strong negative skewness; a central region of approximately zero skewness.

Overall, this gives three general regions: A) a narrow ring near to the wall, with strong positive skewness and high variance; B) a second narrow ring, closer to the centre of the pipe, of strong negative skewness and high variance; and C) a central region where voxels had zero skewness (symmetric) and low variance.

4.2 Serial Phase-Contrast Velocimetry

The rapid serial PC-MRI measurements are shown in Figure 4. In the laminar regime (Q=50ml/min, Re 352; Q137ml/min, Re=966) the PC-MRI measured intravoxel velocity was constant. Around the transition to turbulence (Q=261ml/min, Re 1840), the PC-MRI intravoxel velocity was also constant. In the turbulent regime ((Q=384ml/min, Re 2708), the PC-MRI intravoxel velocity measurements showed random fluctuations, which are particularly broad in the edge and middle voxels

4.3 Accuracy of Phase-Contrast Velocimetry.

Unlike PC-MRI, FFI makes no assumption about the symmetry of intravoxel displacement distributions, hence is not susceptible to symmetry associated errors and can be used as a ground truth. The velocity difference map (PC-MRI mean velocity map subtracted by the FFI mean velocity map), shows where errors in PC-MRI occur due to asymmetric intravoxel distributions (Figure 3f). This revealed three distinct regions: first, a ring adjacent to the wall where PC-MRI underestimated the mean velocity; second, another ring closer in, where PC-MRI over-estimated the mean velocity; and finally, a central region where PC-MRI accurately measured the mean velocity. Using the theoretically derived relationship for velocity error (equation 9), Figure 5 shows how the velocity error depends on q and for a range of values of skewness, variance and kurtosis.

5. Discussion

The theory of PC-MRI assumes that intravoxel displacement distributions are symmetric (24,25). Other approaches like Bayesian multipoint MRI (33) and intravoxel standard deviation (IVSD) also assume a Gaussian displacement distribution. Passable agreement of PC-MRI phantom measurements with both LDA (16) and PIV (19,20) have, to some degree, been taken as validation of this assumption. To investigate the impact of this assumption on the accuracy of PC-MRI, we returned to study the transition to turbulence for non-pulsatile flow through a horizontal pipe.

5.1 Importance of the timescale of intravoxel velocity fluctuations

When there are temporal fluctuations in the intravoxel velocity field, it is important to consider the characteristic timescale of the fluctuations, T_c, compared with MRI timescales: gradient duration δ, the observation time Δ, repetition time TR and total imaging time T_{image} (34,35). For PC-MRI, if the

timescale of fluctuations, T_c, is significantly longer than the imaging time ($T_c > T_{image}$), it is possible to acquire "instantaneous" velocity maps (31,36). For example, in turbulent pipe flow, Sederman et al. were able, with a single excitation, to capture an "instantaneous" velocity map using the GERVAIS method (37). However, in clinical applications of PC-MRI, it is typically necessary to use gradient-echo based sequences, which require multiple excitations to acquire k-space. If fluctuations in the velocity field are rapid compared to the imaging time, ($\delta < T_c < T_{image}$), an averaged intravoxel distribution will be experienced. If this averaged distribution of velocities is asymmetric, PC-MRI will not measure the true mean velocity. Whereas, even with rapid fluctuations ($\delta < T_c < T_{image}$), FFI will measure the true distribution, from which the correct mean velocity can be extracted. In the case of very rapid fluctuations, where T_c is shorter than the gradient duration δ ($T_c < \delta$) it is expected that this would lead to incorrect encoding and signal lose with both PC-MRI and FFI.

5.2 Effect of Turbulent Fluctuations on intravoxel displacement distributions

In our experiments, at the lower flow rates (Q= 50ml/min, Q=137ml/min; Re=352, Re=966 respectively) the flow through the pipe was laminar, showing a parabolic velocity profile. The serial PC-MRI measurements showed constant velocity, indicating no velocity fluctuations. Moreover, the displacement distributions measured by FFI were very narrow (low variance) and symmetric (zero skewness).

At higher flow rates, transitioning to turbulence (Q = 261ml/min, Re= 1840), the velocity profiles showed plug-like flow. The mean velocity maps were not entirely circularly symmetric (Figure 3a,e), which we attribute to slight asymmetries in the pipe, as well as the limited length of straight piping 0.7m before the fluid enters the RF coil. The FFI measured intravoxel displacement distributions near the wall had a much broader range (0-75cm/s) than can be expected from the spread of velocities due to steady flow, which we calculated at a maximum of 20cm/s over a single voxel. Thus, indicating the presence of rapid intravoxel fluctuations, occurring faster than the imaging time ($T_c < T_{image}$) (Figure 2b). The absence of fluctuations in the serial PC-MRI measurements (Figure 4c) indicates that these fluctuations were still slow compared with the encoding time (i.e. $T_c > \delta$).

At the highest flow rate (Q=384ml/min, Re=2708) pipe flow was into the turbulent regime. The serial PC-MRI measurements were no longer constant, showing particular intravoxel fluctuations near the wall (Figure 4d). However, this was still much less than implied by the broad intravoxel velocity distributions seen with FFI. This indicates the fluctuations were even more rapid, probably approaching the encoding timescales of δ and Δ, resulting in PC-MRI encoding errors It should be noted that the FFI measurements appear unaffected by the more rapid fluctuations, as the displacement propagator of the

central voxel is still very narrow at the highest flow rate (Figure 2b). This is probably the result of more signal averaging when acquiring the FFI measurements.

The FFI measurements for laminar flow (Re = 352; Re = 966) showed narrow and symmetric distributions, with FFI measurement of mean intravoxel velocity matching those measured using PC-MRI. However, when transitioning to turbulent flows the picture becomes more complex (Figure 3), with the three distinct bands forming in maps of the higher moments: a ring near the wall, with strong positive skewness and high variance; a second ring, closer in, of strong negative skewness and high variance; and a central region where voxels had zero skewness (symmetric) and low variance. This is qualitatively similar to recent experimental observations using Particle Image Velocimetry, which have confirmed theoretical predictions of unstable traveling waves in turbulent pipe flow at moderate Reynolds numbers (38,39). Here, two distinct regions are seen: high speed streaks were seen in the outer ring of the pipe, which correspond with the region of elevated variance in our experiments (Figure 3b): lower speed streams were seen in the centre of the pipe, corresponding with the central region of low variance in our experiments (fig3b).

5.3 Error in PC-MRI measurements

As discussed in the theory section, unlike PC-MRI, FFI theory makes no assumption about the symmetry of the intravoxel displacement distribution. Hence, we considered the FFI mean velocity maps to be the "ground truth", with the error in PC-MRI velocity maps being the difference between the two (Figure 3f). For laminar flow, the error in the PC-MRI velocity map was negligible. However, as the flow transitions to turbulence (Q=261ml/min, Re=1840) and turbulent flow (Q=384ml/min, Re=2708), velocity errors substantially increased.

With turbulent flow (Q=384ml/min, Re=2708), there are three distinct regions,

1. A ring adjacent the wall, where PC-MRI under-estimates the mean velocity. This region also corresponds to strong positive skewness and high variance.
2. A ring closer in, where PC-MRI over-estimates the mean velocity. This region also corresponds to strong negative skewness and high variance.
3. A central region, where PC-MRI is accurate. This region corresponds to approximately zero skewness and low variance.

The maps of PC-MRI error are not entirely symmetric (Figure 3f). The wall region shows larger underestimation of velocity (darker blue) at the top of the pipe than at the bottom. Further, the second

ring shows larger overestimation of velocity (red) to the right of the pipe than to the left (yellow). This we ascribe to the positioning of the imaging grid relative to the pipe. For example, a voxel by the wall at the top might contain less fluid (more pipe) than the corresponding voxel at the bottom of the pipe. These two voxels will then have different intravoxel displacement distributions, hence different variance and skewness, resulting in different velocimetry errors. For the intermediate flow rate (261ml/min) the same general pattern was discernible in the PC-MRI errors (Figure 3f), however, it is less defined and more asymmetric. This appears to reflect the greater circular asymmetry seen in the mean velocity map at this flow rate from both PC-MRI and FFI measurements.

These experimental results are consistent with our recent theoretical analysis (27), where we derived an analytic expression for PC-MRI errors that resulted from the higher order moments of the displacement. Inspection of equation 9, shows that the skewness of intravoxel displacement distribution has an important effect on the accuracy of PC-MRI measurements. The term V_{error} vanishes for $Skew\big(P_\Delta(R,\boldsymbol{r})\big) = 0$ (accurate mean velocity measurement), becomes negative when $Skew\big(P_\Delta(R,\boldsymbol{r})\big) > 0$ (mean velocity under-estimation) and positive when $Skew\big(P_\Delta(R,\boldsymbol{r})\big) < 0$ (mean velocity over-estimation). Second, the error in PC-MRI measurements, V_{error}, increases with the variance and decreases with the kurtosis of the displacement distribution. Given that this shows the importance of the higher order moments, it is interesting to note that Dyverfeldt *et al* have proposed a framework for their extraction from experimental *q*-space data (40).

A number of studies have described localised regions where PC-MRI can both over-estimate and under-estimates local flow (41) (17,18). It is interesting to note that previous studies validating PC-MRI in turbulent pipe flow, showed good agreement between PC-MRI measured volume flow rates and those measured using a gold standard flowmeter (42) (18,41). Presumably, this results from the cancelling out of regions where PC-MRI over-estimated the true velocity, by regions where it was under-estimated.

However, the bands of over- and under-estimation that we have demonstrated near the pipe wall, will impact PC-MRI measurements of wall shear stress, which depend upon the slope of the velocity profile at the wall. This could be important as PC-MRI measurements of wall-shear stress are now being used clinically to assess the likelihood of carotid plaque or intracranial aneurysms rupturing and leading to stroke (43,44). Our results, showing the over- and under-estimation in PC-MRI measurements near the wall (Figure 3), could result in an over-estimation of wall shear stress in turbulent flow.

In the current experiments there was no detectable signal from the walls of the pipe, however, in other PC-MRI applications this may not be the case. For example, in clinical applications there is signal originating from water molecules diffusing in the wall tissue of blood vessels. In such a case, where a voxel covers both the wall (non-flowing diffusion) and the flowing fluid, this can increase both the variance and skewness of the resulting intravoxel displacement distribution, thus increasing potential velocimetry errors close to the wall.

It is interesting to note a previous investigation of PC-MRI errors, which studied the turbulent jets formed in a stenotic phantom (a straight pipe, containing a circular plate, with a concentric circular orifice (41). For a fixed Venc, it was found that the PC-MRI errors were reduced with decreasing echo time, TE , which corresponds to a decreased observation time. We believe these results can be readily explained by considering the asymmetry of the intravoxel displacement distribution As described above, in the case where ($\delta < T_c < T_{\text{image}}$), decreasing the observation time results in reduced skewness and variance of the intravoxel distribution, hence reduced PC-MRI errors. Finally, it is worth noting that the above discussions do not preclude other sources of PC-MRI errors. For example, in turbulent fluctuations acceleration will be present, which may also affect the accuracy of PC-MRI measurements.

5.4 Minimising velocimetry errors

It is important to note that PC-MRI velocimetry errors, V_{error}, depend on the chosen experimental parameters, namely q and Δ (cf. equation 9). With regard to observation time Δ, errors will generally be minimised by choosing the smallest achievable value of Δ, as this will minimise the skewness and variance of the intravoxel displacement distributions. With regard to q, it is worth considering how this parameter is often chosen in velocimetry experiments. Commonly, the value of q is calculated from an estimated maximum velocity (Venc), setting the resultant phase shift for this velocity to be π, giving

$$V_{enc} = \frac{\pi}{(q_2 - q_1)\Delta} \qquad (10)$$

However, it should be noted that for voxels with asymmetric distributions, this choice of q will maximise the error. Generally, these errors may be reduced by using a lower value of *q (i.e. choosing a larger* V_{enc}*),* (Figure 5). As discussed previously (27), this type of error can be intuitively appreciated by considering its geometric origin. In PC-MRI the assumption of symmetric distributions implies that the phase of the NMR signal is equivalent to the average phase of the individual spin phases φ_i ,

$$\varphi_{average} = \frac{\sum_{i=1}^{n} \varphi_i}{n}, \qquad (11)$$

Whereas, the actual phase measured in NMR experiments is the resultant phase from the vector addition of all the individual spin vectors, φ_{vector},

$$\varphi_{vector} = tan^{-1}\left(\frac{\sum_{i=1}^{n} sin\, \varphi_i}{\sum_{i=1}^{n} cos\, \varphi_i}\right). \qquad (12)$$

The phase error is the difference between the two ($\varphi_{error} = \varphi_{vector} - \varphi_{average}$). Figure 6 shows a simple example of this using a positively skewed distribution of 3 unit vectors, where using half the value of q results in substantially less phase error. However, it should also be noted that at lower *q,* the resultant phase shift is reduced, leading to an increased contribution from noise related phase errors.

6. Conclusion

We have demonstrated experimentally that the assumption of symmetric intravoxel displacement distributions made in PC-MRI theory, may not be valid for unsteady flows. In a horizontal straight pipe, turbulent intravoxel fluctuations in the velocity field can result in broad asymmetric displacement distributions. This can lead to either an under-estimation or an over-estimation of the true mean intravoxel velocity. These experimental results are consistent with our theoretical analysis, in which PC-MRI errors are a function of the higher moments of the intravoxel displacement distribution and the experimental parameters (q, Δ). Further, this indicates that this type of PC-MRI errors may be reduced by using lower q values or a shorter observation time Δ (i.e. higher V_{ENC}).

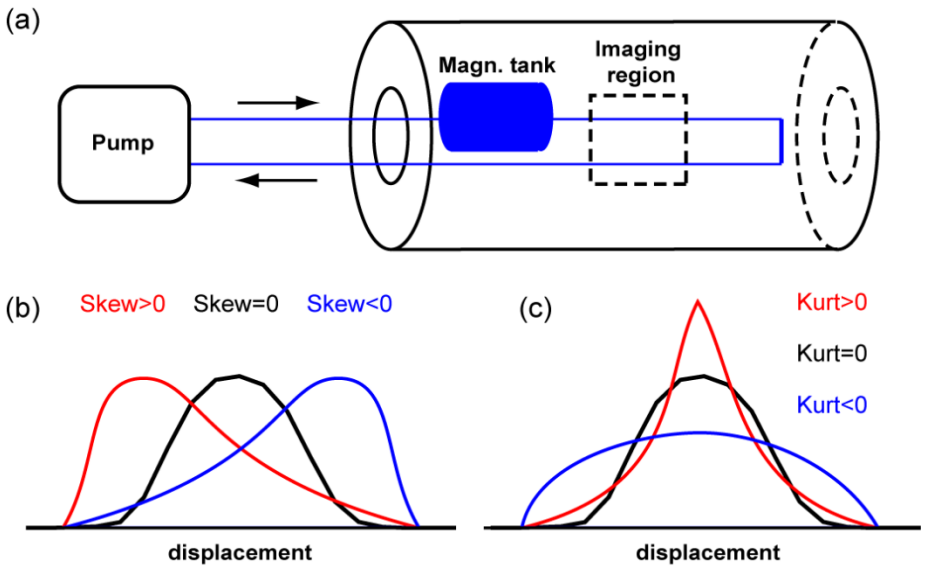

Figure 1: a) Schematic of experimental set-up. Due to fast flow a reservoir of water was placed inside the magnet to ensure full polarization; b) Schematic diagram of the relationship of skewness to the distribution shape; (c) Schematic diagram of the relationship of kurtosis to the distribution shape.

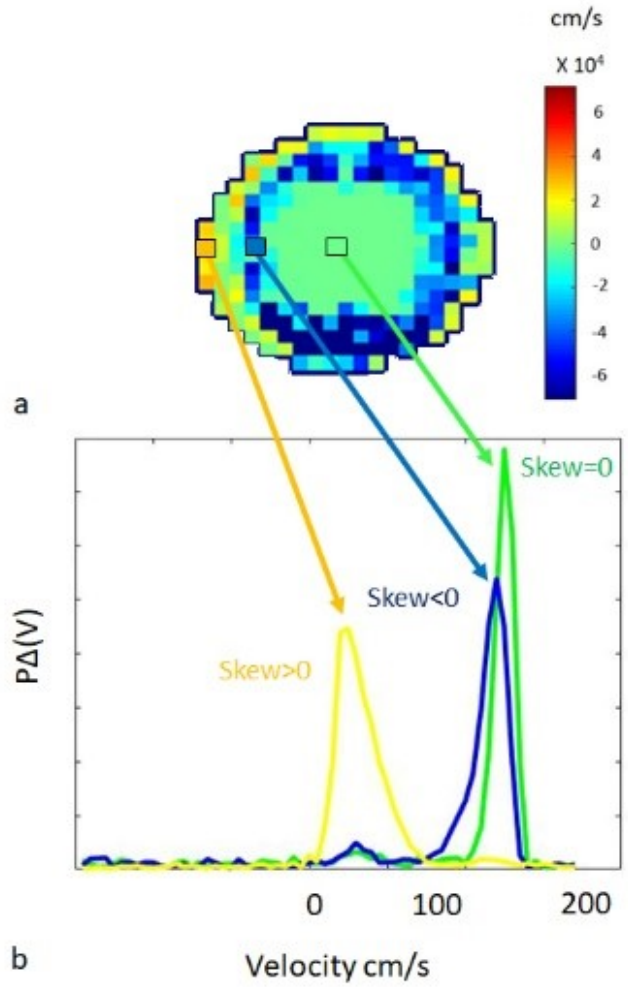

Figure 2: a) Skewness map from FFI (flowrate 261 ml/min); b) Example of velocity distribution from selected voxels. The wall voxel (yellow) shows positive skewness and high variance. The second ring closer in (blue) shows negative skewness and high variance. The central voxel (green) shows zero skewness and low variance.

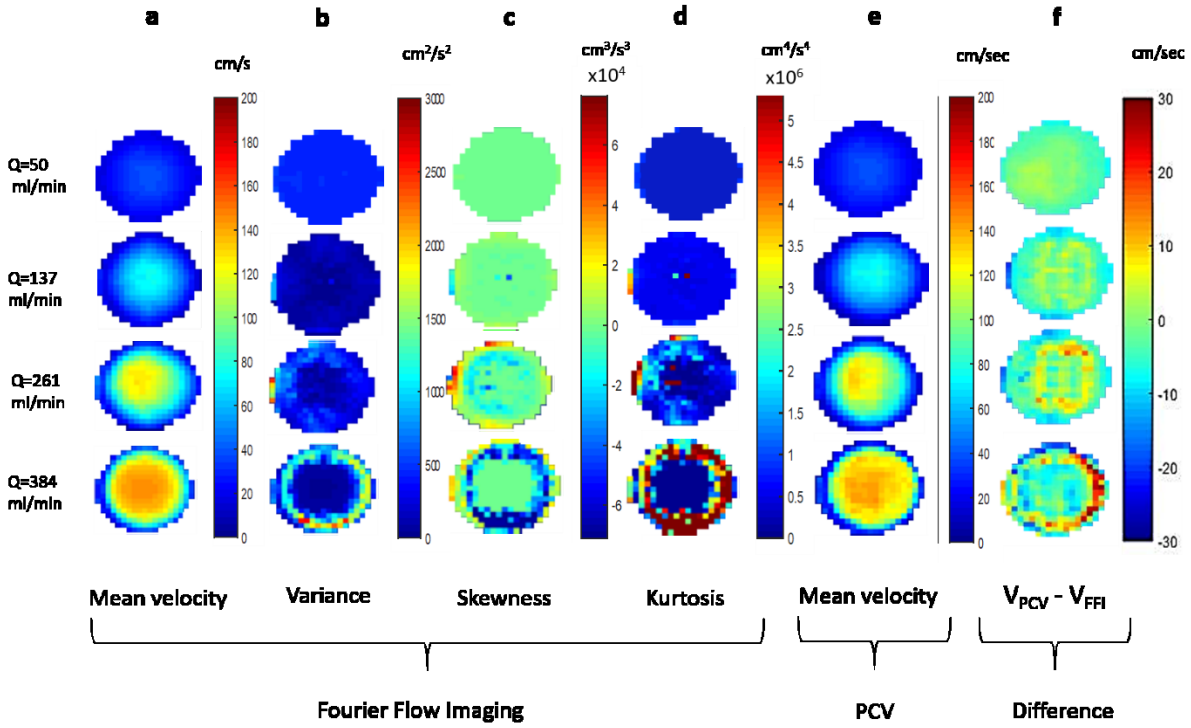

Figure 3: PC-MRI and FFI results for three different flow rates. For each FFI voxel the moments of the displacement distribution were calculated, giving spatial maps of the mean (a), variance (b), skewness (c) and kurtosis (d). Column (e) shows mean velocity measured by PC-MRI. Column (f) shows the difference between mean velocity measured by PC-MRI and FFI.

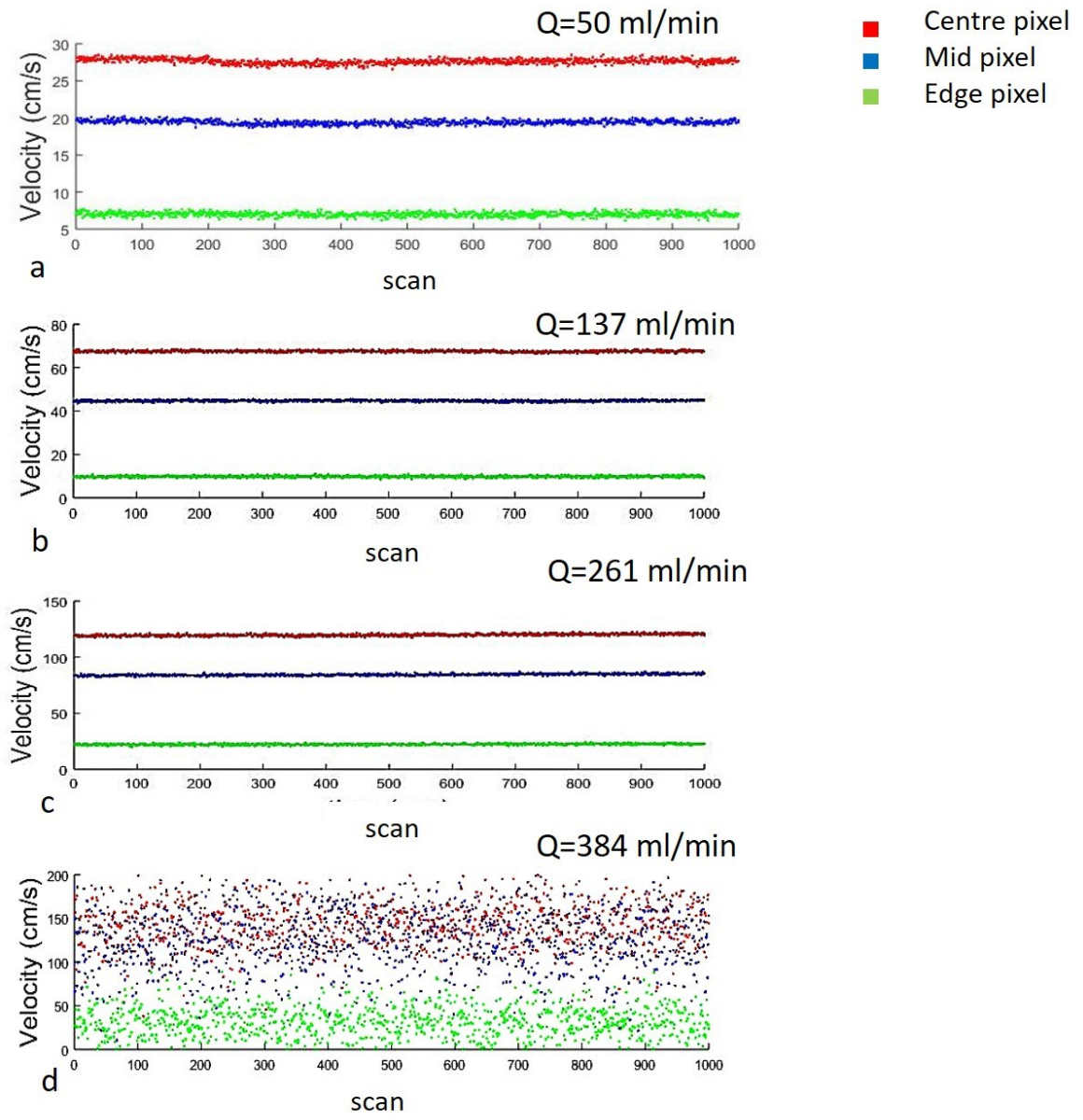

Figure 4. The rapid serial PC-MRI measurements. A) In the laminar regime (Q=50ml/min, Re 352; Q137ml/min, Re=966) the PC-MRI measured intravoxel velocities were constant. Around the transition to turbulence (Q=261ml/min, Re 1840), the PC-MRI intravoxel velocity were also constant. In the turbulent regime ((Q=384ml/min, Re 2708), the PC-MRI intravoxel velocity measurements showed random fluctuations, which are particularly broad in the edge and middle voxels

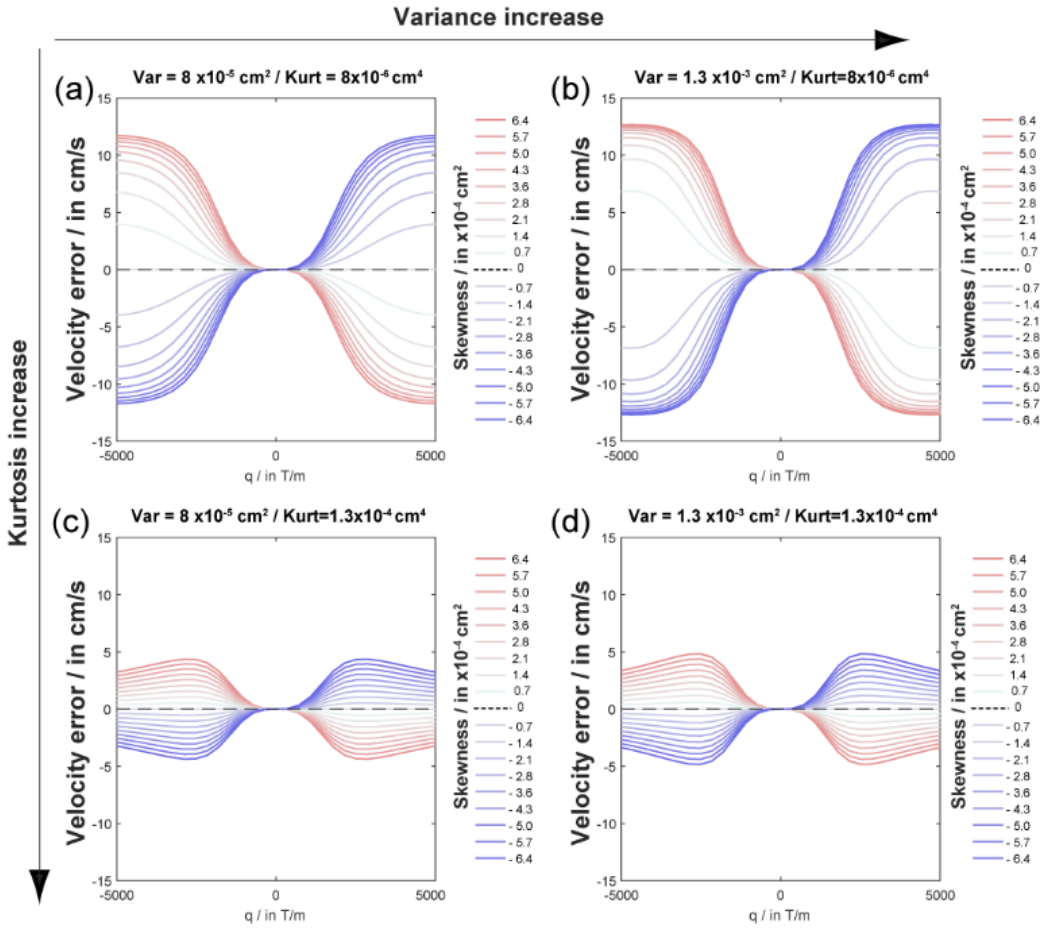

Figure 5. Skewness effect on theoretical velocity error against q (calculated using equation 9) for the minimum and maximum values of kurtosis and variance observed in the experimental data presented in this work and for the same skewness range.

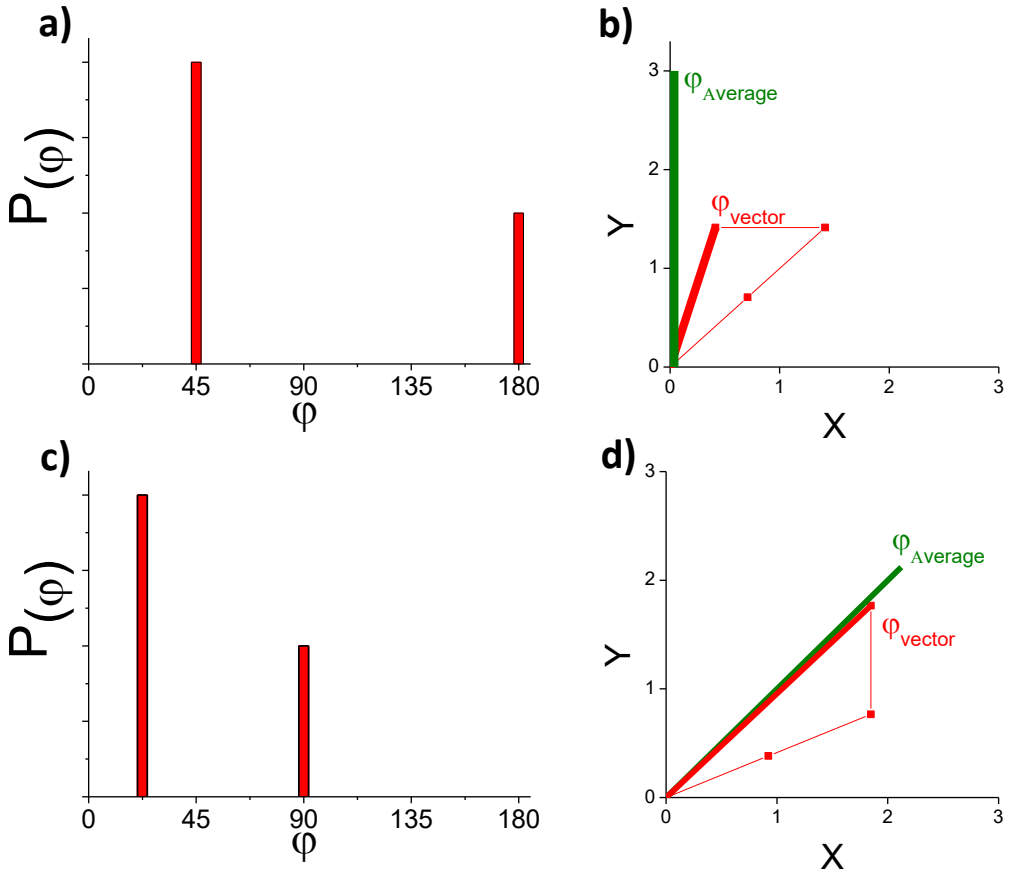

Figure 6 Simple illustration of how PC-MRI errors from asymmetric distributions can be reduced by selecting a lower q value. a) Consider a positively skewed distribution $P(\varphi)$ of three unit vectors (phase 45°, 45° and 180°), where the q value was selected to give the fastest a phase of 180°. b) This distribution results in a larger difference between the average of the individual phases, $\varphi_{average}$, and the phase from vector addition, φ_{vector}, i.e. a large PC-MRI error. c) Halving the applied q value (i.e. doubling the V_{enc}) results in phases of 22.5°, 22.5° and 90°. d) This results is a substantially smaller difference between $\varphi_{average}$ and φ_{vector}, i.e. more accurate PC-MRI.

REFERENCES

1. Gatehouse PD, Keegan J, Crowe LA, Masood S, Mohiaddin RH, Kreitner KF, Firmin DN. Applications of phase-contrast flow and velocity imaging in cardiovascular MRI. Eur Radiol 2005;15(10):2172-2184.
2. Elkins CJ, Alley MT. Magnetic resonance velocimetry: applications of magnetic resonance imaging in the measurement of fluid motion. Exp Fluids 2007;43(6):823-858.
3. Hayward RJ, Tomlinson DJ, Packer KJ. Pulsed Field-Gradient Spin-Echo NMR Studies of Flow in Fluids. Mol Phys 1972;23(6):1083-+.
4. Moran PR. A Flow Velocity Zeugmatographic Interlace for NMR Imaging in Human Body. Magn Reson Imaging 1982;1(197):197-203.
5. Caprihan A, Altobelli SA, Benitez-Read E. Flow-Velocity Imaging from Linear-Regression of Phase Images with Techniques for Reducing Eddy-Current Effects. J Magn Reson 1990;90(1):71-89.
6. Axel L, Morton D. MR Flow Imaging by Velocity-Compensated/Uncompensated Difference Images. J Comput Assist Tomogr 1987;11(1):31-34.
7. Ha H, Ziegler M, Welander M, Bjarnegard N, Carlhall CJ, Lindenberger M, Lanne T, Ebbers T, Dyverfeldt P. Age-Related Vascular Changes Affect Turbulence in Aortic Blood Flow. Front Physiol 2018;9.
8. Humphrey JD, Schwartz MA, Tellides G, Milewicz DM. Role of Mechanotransduction in Vascular Biology: Focus on Thoracic Aortic Aneurysms and Dissections. Circ Res 2015;116(8):1448-1461.
9. Wang L, Luo JY, Li BC, Tian XY, Chen LJ, Huang YH, Liu J, Deng D, Lau CW, Wan S, Ai D, Mak KLK, Tong KK, Kwan KM, Wang NP, Chiu JJ, Zhu Y, Huang Y. Integrin-YAP/TAZ-JNK cascade mediates atheroprotective effect of unidirectional shear flow. Nature 2016;540(7634):579-+.
10. Yoganathan AP, Woo YR, Sung HW. Turbulent Shear-Stress Measurements in the Vicinity of Aortic Heart-Valve Prostheses. J Biomech 1986;19(6):433-442.
11. Kuethe DO, Gao JH. NMR signal loss from turbulence: Models of time dependence compared with data. Physical Review E 1995;51(4):10.
12. Li TQ, Seymour JD, Powell RL, McCarthy KL, Odberg L, McCarthy MJ. Turbulent pipe flow studied by time-averaged NMR imaging measurements of velocity profiles and turbulent intensity. Magn Reson Imaging 1994;12(6):11.
13. Ziegler M, Lantz J, Ebbers T, Dyverfeldt P. Assessment of Turbulent Flow Effects on the Vessel Wall Using Four-Dimensional Flow MRI. Magn Reson Med 2017;77(6):2310-2319.
14. Siegel JM, Oshinski JN, Pettigrew RI, Ku DN. The accuracy of magnetic resonance phase velocity measurements in stenotic flow. J Biomech 1996;29(12):1665-1672.
15. Hollnagel DI, Summers PE, Kollias SS, Poulikakos D. Laser Doppler velocimetry (LDV) and 3D phase-contrast magnetic resonance angiography (PC-MRA) velocity measurements: Validation in an anatomically accurate cerebral artery aneurysm model with steady flow. J Magn Reson Imaging 2007;26(6):1493-1505.
16. Dyverfeldt P, Sigfridsson A, Kvitting JPE, Ebbers T. Quantification of intravoxel velocity standard deviation and turbulence intensity by generalizing phase-contrast MRI. Magn Reson Med 2006;56(4):850-858.
17. van Ooij P, Guedon A, Poelma C, Schneiders J, Rutten MCM, Marquering HA, Majoie CB, vanBavel E, Nederveen AJ. Complex flow patterns in a real-size intracranial aneurysm phantom: phase contrast MRI compared with particle image velocimetry and computational fluid dynamics. NMR Biomed 2012;25(1):14-26.
18. Khodarahmi I, Shakeri M, Kotys-Traughber M, Fischer S, Sharp MK, Amini AA. In Vitro Validation of Flow Measurement With Phase Contrast MRI at 3 Tesla Using Stereoscopic

Particle Image Velocimetry and Stereoscopic Particle Image Velocimetry-Based Computational Fluid Dynamics. J Magn Reson Imaging 2014;39(6):1477-1485.
19. Adrian RJ. Twenty years of particle image velocimetry. Exp Fluids 2005;39(2):159-169.
20. Elkins CJ, Alley MT, Saetran L, Eaton JK. Three-dimensional magnetic resonance velocimetry measurements of turbulence quantities in complex flow. Exp Fluids 2009;46(2):285-296.
21. Frayne R, Steinman DA, Ethier CR, Rutt BK. Accuracy of MR Phase-Contrast Velocity-Measurements for Unsteady-Flow.J Magn Reson Im 1995;5(4):428-431.
22. Petersson S, Dyverfeldt P, Gardhagen R, Karlsson M, Ebbers T. Simulation of Phase Contrast MRI of Turbulent Flow. Magn Reson Med 2010;64(4):1039-1046.
23. Shokina N, Bauer A, Teschner G, Buchenberg WB, Tropea C, Egger H, Hennig J, Krafft AJ. MR-based wall shear stress measurements in fully developed turbulent flow using the Clauser plot method. J Magn Reson 2019;305:16-21.
24. Hamilton CA, Moran PR, Santago P, Rajala SA. Effects of Intravoxel Velocity Distributions on the Accuracy of the Phase-Mapping Method in Phase-Contrast MR-Angiography. J Magn Reson Imaging 1994;4(5):752-755.
25. Wolf RL, Ehman RL, Riederer SJ, Rossman PJ. Analysis of Systematic and Random Error in MR Volumetric Flow Measurements. Magn Reson Med 1993;30(1):82-91.
26. Shukla MN, Vallatos A, Phoenix VR, Holmes WM. Accurate phase-shift velocimetry in rock. J Magn Reson 2016;267:43-53.
27. Vallatos A, Al-Mubarak HFI, Mullin JM, Holmes WM. Accuracy of phase-contrast velocimetry in systems with skewed intravoxel velocity distributions. J Magn Reson 2018;296:121-129.
28. Vallatos A, Shukla MN, Mullin JM, Phoenix VR, Holmes WM. The effect of displacement distribution asymmetry on the accuracy of phase-shift velocimetry in porous media. Micropor Mesopor Mat 2018;269:130-133.
29. Reynolds O. An experimental investigation of the circumstances which determine whether the motion of water shall be direct or sinuous, and of the law of resistance in parallel channels. Proc R Soc London 1883;35(54), 935-982
30. Coulson JM, Richardson JF. Chemical Engineering: Fluid Flow, Heat and Mass Transfer. oxford: Butterworth-Heinemann; 1996.
31. Lopez-Gonzalez MR, Holmes WM, Callaghan PT. Rheo-NMR phenomena of wormlike micelles. Soft Matter 2006;2(10):855-869.
32. Dumoulin CL, Hart HR. Magnetic-Resonance Angiography. Radiology 1986;161(3):717-720.
33. Knobloch V. Mapping mean and fluctuating Velocities by multipoint MR velocity encoding. Magn Reson Med 2014;71:10.
34. Callaghan PT. Translational Dynamics and Magnetic Resonance: Principles of Pulsed Gradient Spin Echo NMR: Oxford University Press; 2011.
35. Gatenby JC, Gore JC. Characterization of turbulent flows by NMR measurments with pulsed gradients. Journal of Magnetic Resonance, series a 1994;110:6.
36. Lopez-Gonzalez MR, Holmes WM, Callaghan PT, Photinos PJ. Shear banding fluctuations and nematic order in wormlike micelles. Phys Rev Lett 2004;93(26).
37. Sederman AJ, Mantle MD, Buckley C, Gladden LF. MRI technique for measurement of velocity vectors, acceleration, and autocorrelation functions in turbulent flow. J Magn Reson 2004;166(2):182-189.
38. Hof B, van Doorne CWH, Westerweel J, Nieuwstadt FTM, Faisst H, Eckhardt B, Wedin H, Kerswell RR, Waleffe F. Experimental observation of nonlinear traveling waves in turbulent pipe flow. Science 2004;305(5690):1594-1598.
39. Hof B, van Doorne CWH, Westerweel J, Nieuwstadt FTM. Turbulence regeneration in pipe flow at moderate Reynolds numbers. Phys Rev Lett 2005;95(21).
40. Dyverfeldt P, Sigfridsson A, Knutsson H, Ebbers T. A Novel MRI Framework for the Quantification of Any Moment of Arbitrary Velocity Distributions. Magn Reson Med 2011;65(3):725-731.

41. O'Brien KR, Cowan BR, Jain M, Stewart RAH, Kerr AJ, Young AA. MRI phase contrast velocity and flow errors in turbulent stenotic jets. J Magn Reson Imaging 2008;28(1):210-218.
42. Lee J, Ko S, Cho JH, Song S. Validation of magnetic resonance velocimetry for mean velocity measurements of turbulent flows in a circular pipe. J Mech Sci Technol 2017;31(3):1275-1282.
43. Barker AJ, Lanning C, Shandas R. Quantification of haemodynamic wall shear stress in patients with bicuspid aortic valve using phase-contrast MRI. Ann Biomed Eng 2010;38(3):22.
44. Boussel L, Martin A, Lawton M, Higashida R, Saloner D. Phase-Contrast Magnetic Resonance Imaging Measurements in Intracranial Aneurysms In Vivo of Flow Patterns, Velocity Fields, and Wall Shear Stress: Comparison with Computational Fluid Dynamics Magn Reson Med 2009;61(2):8.